# Using a Flexibility Constrained 3D Statistical Shape Model
# for Robust MRF-Based Segmentation

Tahir Majeed[1]     Ketut Fundana[1]     Marcel Lüthi[2]     Silja Kiriyanthan[1]     Jörg Beinemann[3]
Philippe C. Cattin[1]

[1]Medical Image Analysis Center, University of Basel, Switzerland

{tahir.majeed,ketut.fundana,silja.kiriyanthan,philippe.cattin}@unibas.ch

[2]Computer Science Department, University of Basel, Switzerland

marcel.luethi@unibas.ch

[3]Hightech Research Center of CMF Surgery, University Hospital Basel, Switzerland

jbeinemann@uhbs.ch

## Abstract

*In this paper we propose a novel segmentation method that integrates prior shape knowledge obtained from a 3D statistical model into the Markov Random Field (MRF) segmentation framework to deal with severe artifacts, noise and shape deformations. The statistical model is learned using a Probabilistic Principal Component Analysis (PPCA), which allows us to reconstruct the optimal shape and to compute the remaining variance of the statistical model from partial information. The statistical model, with its remaining variance, can then be used to constrain the shape space, which is a more efficient shape update as compared to a regularization-based shape model reconstruction. The reconstructed shape is optimized over an edge weighted unsigned distance map calculated from the current segmentation, and is then used as a shape prior for the next iteration of the segmentation. We show the robustness to high-density imaging artifacts of the proposed method by providing a quantitative and qualitative evaluation to the challenging problem of 3D masseter muscles segmentation from CT datasets.*

## 1. Introduction

Face is the unique external perceivable identity of a human. It depicts the individual personality and the characteristics of the human in daily contact with other humans thus making it of fundamental importance for them. It is the area where most of the important sense organs are present. These sense organs are the main source for conveying our expressions to others. The shape and the unique features of a face are determined by the musculoskeletal system which



(a) Side view.     (b) Frontal view.     (c) Axial view.
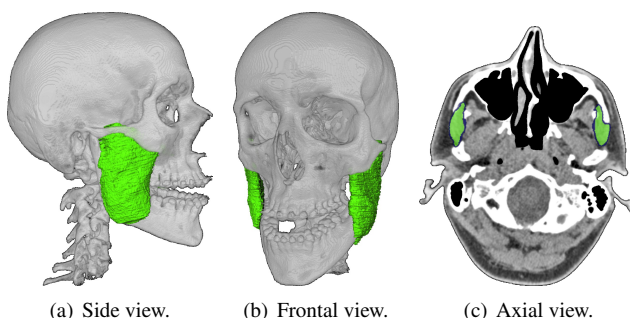
Figure 1. (a,b) 3D and (c) 2D views of the masseter muscle (green) (color online).

consists of bones and soft tissues. For any facial surgical treatment accurate planning based on available preoperative diagnostic datasets, such as segmentation of bones and soft tissues, is important to guarantee an optimal, functional and aesthetical outcome.

Image segmentation is an ill-posed problem which aims to separate a given image into at least two constituent parts. This problem can be solved by using MRFs in which efficient optimization methods, such as graph-cuts [4] can be used to find the global minimum that is based only on the low-level prior knowledge encoded into the regional and boundary terms of the energy functional. Datasets corrupted by imaging artifacts, inhomogeneities or noise require additional shape information in order to efficiently constrain the target anatomical structure. The main challenges, however, lies in integrating diverse prior information into graph-cuts and in modeling the shape variability.

There are two fundamental approaches to integrate the shape priors. Either they are integrated into the boundary
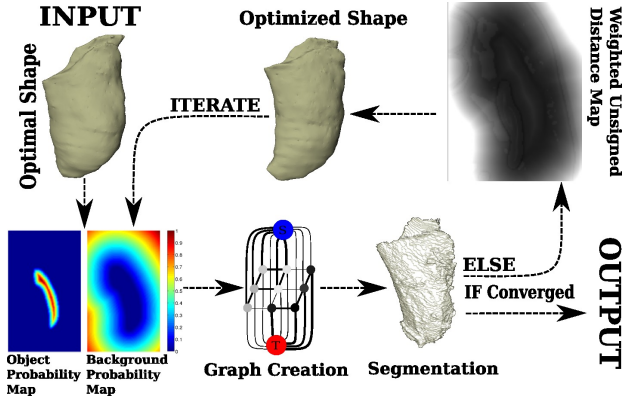
Figure 2. Segmentation process (color online).

term of the MRF, such as in Das *et al.* [7], Freedman and Zhang [10] and Veksler [17], or into the regional term of the MRF, such as in Slabaugh and Unal [15], El-Zehiry and Elmaghraby [9], Ali *et al.* [1], Freiman *et al.* [11], Malcolm *et al.* [14].

Modeling shape variability is crucial in order to obtain desired solutions, especially in medicine where anatomical structures have considerable shape variability. Some methods, such as the elliptical shape prior of Slabaugh and Unal [15], the compact shape prior of Das *et al.* [7] and star shape priors of Veksler [17] have the drawback that the class of representable shapes is limited. Freedman and Zhang [10] used an unsigned distance map of the aligned shape template's contour represented by the 0-level set to incorporate prior shape knowledge. Although there is no restriction on the types of shapes that can be represented, their method requires a good initial alignment of a fixed template with the object of interest. A fixed shape template is not versatile enough to capture the shape variability generally seen in anatomical structures. El-Zehiry and Elmaghraby [9], Ali *et al.* [1], Freiman *et al.* [11] and Malcolm *et al.* [14] incorporated statistically learned shape models. El-Zehiry and Elmaghraby, Ali *et al.* and Freiman *et al.* learned their shape models by registering the training shapes and then creating a probability map by over-laying the registered shapes. The problem with such methods is that there is no statistical dependence between the shapes, where certain invalid shapes can be generated from such models. To elevate the problem of possibly generating invalid shapes, Malcolm *et al.* [14] learned the shape model through the application of kernel PCA.

As automatic segmentation with MRF is prone to leaking due to weak edges, noise, imaging artifacts and the missing shape knowledge, we developed a novel approach that combines MRF-based segmentation with a 3D statistical shape model as prior anatomical knowledge. The shape model is constructed from the manually segmented CT datasets by using a linear PCA to model the shape variability. Instead of constraining the variability of the model through regularization [2, 18], where finding a good regularization parameter for all datasets is difficult, we adapt the constrained variability approach of Lüthi *et al.* [12]. The variability can be constrained by additional observed knowledge, such as input landmarks. In segmenting the masseter muscle (see Fig. 1), for instance, the muscle attachments to the bone, as well as a previous skull segmentation step, can be used as landmarks. Our segmentation process is done as follows: First we use an initial shape generated using the statistical model that best fits the landmarks, as the starting shape prior to segment the muscle. We then use the result to reconstruct a new optimal shape prior using the statistical model for the next iteration. This process is repeated until convergence as shown in Fig. 2.

The main advantages of the proposed method are efficient ways: 1) to integrate a 3D shape model into the regional term of the graph-cut; 2) to constrain the shape model to maximize the robustness with respect to noise, artifacts and shape degeneration; 3) to iteratively optimize the shape prior and intensity profile based on the evidence from the previous segmentation which increases the segmentation accuracy.

## 2. Statistical Model

Statistical shape models are widely used to capture the shape variability of a class of shapes from a representative set of training shapes [6, 18]. If the training dataset is a good representative of the class of shapes, then the resulting statistical model can be fitted to any shape within this class.

In our work the shape knowledge is learned from the PPCA based approach as suggested by Lüthi *et al.* [12] instead of using the traditional PCA based approach of [6, 18]. The difference is that PPCA provides an additional probabilistic interpretation of the PCA based model. The main assumption while building statistical shape models is that the samples are Independent and Identically Distributed (i.i.d) having a multivariate Gaussian distribution with probability density function $p \sim \mathcal{N}(\bar{\mathbf{x}}, \mathbf{\Sigma})$ with mean $\bar{\mathbf{x}}$ and covariance $\mathbf{\Sigma}$. Singular Value Decomposition (SVD) can then be applied to decompose $\mathbf{\Sigma} = \mathbf{U}\mathbf{D}^2\mathbf{U}^T$. $\mathbf{U}$ are the eigenvectors while $\mathbf{D}^2$ represents the corresponding eigenvalues of $\mathbf{\Sigma}$. Let $\{\mathbf{x}^i \in \mathbb{R}^{3m} | i = 1, \dots, n\}$ be $n$ 3D triangulated surface meshes where $m$ is the number of vertices. Shape $\mathbf{x}^1$ is arbitrarily chosen as the reference surface. All the surfaces are aligned with $\mathbf{x}^1$ by aligning the manually labeled landmarks on the sample shapes $\mathbf{x}^i$ using procrustes alignment. $\mathbf{x}^i$ are then registered with $\mathbf{x}^1$ by computing curvature sensitive deformation fields for the vertices of $\mathbf{x}^1$ using the method of Dedner *et al.* [8], which results in all sample shapes having the same number of vertices. The goal is to build a statistical shape model of the muscle over this distribution of surface meshes using the PPCA based approach.

## 2.1. Reconstruction from Partial Information

A surface mesh $\mathbf{x}$ can be partitioned into $\mathbf{x} := (\mathbf{x}_a, \mathbf{x}_b)^T$, where $\mathbf{x}_b \in \mathbb{R}^{3l}$ is the known information based on $l$-landmarks while $\mathbf{x}_a$ is unknown and which is to be estimated from the known information. We assume that this additional knowledge is provided in the form of $l$-landmark points. In our application these landmarks are obtained from manually labeled landmarks, which in our case are the muscle attachments at the facial bones. Once $\mathbf{x}_b$ is known, it is natural to assume that the total variability of the statistical model will reduce as further evidence is obtained. The probability distribution of shape $\mathbf{x}$ can be written as

$$p(\mathbf{x}) = p(\mathbf{x}_a, \mathbf{x}_b) = \mathcal{N}\left(\begin{bmatrix} \bar{\mathbf{x}}_a \\ \bar{\mathbf{x}}_b \end{bmatrix}, \begin{bmatrix} \mathbf{W}_a \mathbf{W}_a^T & \mathbf{W}_a \mathbf{W}_b^T \\ \mathbf{W}_b \mathbf{W}_a^T & \mathbf{W}_b \mathbf{W}_b^T \end{bmatrix} + \sigma^2 \mathcal{I}_{3l}\right), \quad (1)$$

where $\mathcal{I}_{3l}$ is a $3l \times 3l$ identity matrix, $\mathbf{W} = [\mathbf{W}_a \mathbf{W}_b]^T \in \mathbb{R}^{3m \times d}$ is the $d$-largest scaled eigenvectors and $\sigma$ is a parameter that controls the remaining variance of the statistical model. As it is assumed that $\mathbf{x}$ has a multivariate normal distribution, the conditional distribution $p(\mathbf{x}_a|\mathbf{x}_b) \sim \mathcal{N}(\bar{\mathbf{x}}_{\mathbf{x}_a|\mathbf{x}_b}, \mathbf{\Sigma}_{\mathbf{x}_a|\mathbf{x}_b})$ is also a multivariate normal distribution with mean $\mathbf{x}_{\mathbf{x}_a|\mathbf{x}_b}$ and covariance $\mathbf{\Sigma}_{\mathbf{x}_a|\mathbf{x}_b}$.

It is however, not possible to compute $\mathbf{\Sigma}_{\mathbf{x}_a|\mathbf{x}_b}$ directly since it is potentially huge. As the shape $\mathbf{x}$ can be determined from $\boldsymbol{\alpha}$, the coefficients of the main modes of variation of the statistical model, and the distribution of $\boldsymbol{\alpha}$ in turn can be estimated from the partial information $\mathbf{x}_b$ as $p(\boldsymbol{\alpha}|\mathbf{x}_b)$. It is known that

$$p(\mathbf{x}_b|\boldsymbol{\alpha}) = \mathcal{N}(\mathbf{W}_b \boldsymbol{\alpha} + \bar{\mathbf{x}}_b, \sigma^2 \mathcal{I}_{3l}), \quad (2)$$

and since $p(\boldsymbol{\alpha}) \sim \mathcal{N}(0, \mathcal{I}_d)$, then using the Theorem of the Linear Gaussian Model [2]

$$p(\boldsymbol{\alpha}|\mathbf{x}_b) = \mathcal{N}(\mathbf{M}^{-1} \mathbf{W}_b^T \sigma^{-2}(\mathbf{x}_b - \bar{\mathbf{x}}_b), \mathbf{M}^{-1}), \quad (3)$$

where $\mathbf{M} = \sigma^{-2} \mathbf{W}_b^T \mathbf{W}_b + \mathcal{I}_d$.

Once $\boldsymbol{\alpha}$ is determined the most likely reconstructed shape $\mathbf{x}^*$ given partial shape information $\mathbf{x}_b$ can be calculated using

$$\mathbf{x}_{\mathbf{x}_a|\mathbf{x}_b} = \mathbf{x}^* = \arg \max_x p(\mathbf{x}|\boldsymbol{\alpha}) = \mathbf{W}\boldsymbol{\alpha} + \bar{\mathbf{x}}. \quad (4)$$

Here $\mathbf{x}^*$ also happens to be the mean shape $\bar{\mathbf{x}}_{\mathbf{x}_a|\mathbf{x}_b}$ of the statistical model with constrained variability.

Larger $\sigma$ means higher remaining variance and the landmarks are allowed to deviate more from the marked locations. On the other hand, smaller $\sigma$ means lower variance and the landmarks stay closer to the marked locations but then the model undergoes over fitting. The maximum likelihood estimates of $\bar{\mathbf{x}}, \mathbf{W}, \sigma$ can be calculated as shown by Tipping and Bishop [16].



(a) Original variance.  (b) Remaining variance.
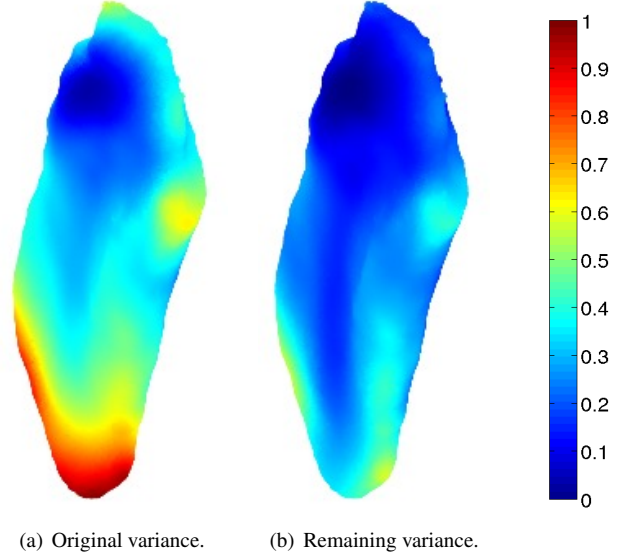
Figure 3. Normalized variances of the statistical model (color online).

## 2.2. Remaining Variance

The covariance matrix $\mathbf{\Sigma}_{\mathbf{x}_a|\mathbf{x}_b}$ can be decomposed as

$$\mathbf{W}\mathbf{M}^{-1}\mathbf{W}^T$$
$$= \mathbf{U}_d \{\underbrace{(\mathbf{D}_d^2 - \sigma^2 \mathcal{I}_d)^{\frac{1}{2}} \mathbf{M}^{-1} (\mathbf{D}_d^2 - \sigma^2 \mathcal{I}_d)^{\frac{1}{2}}}_{\mathbf{A}}\} \mathbf{U}_d^T. \quad (5)$$

As it is prohibitively large, Lüthi *et al.* [12] suggest applying SVD on $\mathbf{A}$, that is,

$$\mathbf{SVD}(\mathbf{A}) := \tilde{\mathbf{U}} \mathbf{D}_{\mathbf{x}_a|\mathbf{x}_b}^2 \tilde{\mathbf{U}}^T. \quad (6)$$

Thus we have an eigenvalue decomposition

$$\mathbf{W}\mathbf{M}^{-1}\mathbf{W}^T = (\mathbf{U}_d \tilde{\mathbf{U}}) \, \mathbf{D}_{\mathbf{x}_a|\mathbf{x}_b}^2 \, (\mathbf{U}_d^T \tilde{\mathbf{U}}^T), \quad (7)$$

where $\mathbf{U}_d \tilde{\mathbf{U}}$ is the orthogonal principal components and $\mathbf{D}_{\mathbf{x}_a|\mathbf{x}_b}^2$ is the diagonal matrix of the corresponding variances. $\mathbf{U}_d \tilde{\mathbf{U}}$, $\mathbf{D}_{\mathbf{x}_a|\mathbf{x}_b}^2$ and $\mathbf{x}^*$ can now be used to generate a new shape $\mathbf{x}$ with the remaining flexibility of the model using

$$\mathbf{x} = \mathbf{x}^* + (\mathbf{U}_d \tilde{\mathbf{U}}) \mathbf{D}_{\mathbf{x}_a|\mathbf{x}_b} \boldsymbol{\alpha}. \quad (8)$$

As an illustration of the concept of remaining variability, we show in Fig. 3 the original variance of the model (a) and the remaining variance of the model after being fit to the muscle attachments (b). For in-depth analysis of the reconstruction of a complete shape given partial information and calculating the remaining variance see Lüthi *et al.* [12].
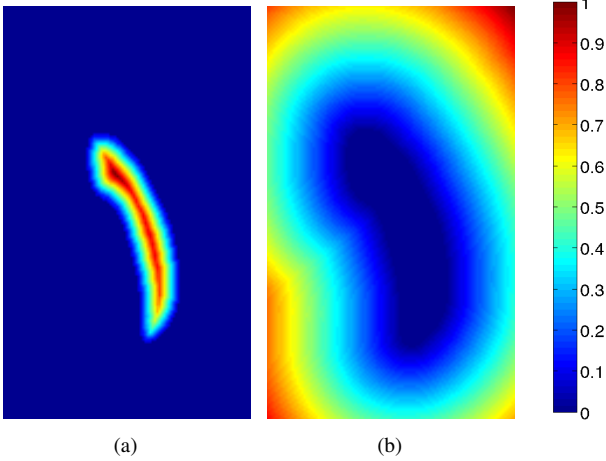
Figure 4. The probability maps of the object (a) and the background (b) (color online).

## 3. Segmentation Model

The MRF theory provides a nice mathematical framework for solving image segmentation problems, which can be casted as a binary labeling problem. Minimizing the energy of this binary labeling results in the segmentation of the target structure. Let $\mathcal{P} = \{1, 2, ...Y\}$ be the set of $Y$ voxels of the volume dataset and let a neighborhood system $\mathbb{N} = \{N_p | \forall p \in \mathcal{P}\}$ defined over the set of voxels $\mathcal{P}$, where $N_p$ consists of all unordered 26 neighbors of the voxel $p \in \mathcal{P}$. Let $\mathcal{Z} = \{z_1, z_2\} = \{0, 1\}$ be the set of binary labels, 0 for background and 1 for object. The goal of the image segmentation problem is to find an optimal mapping $\phi : \mathcal{P} \longmapsto \mathcal{Z}$ that assigns a label from $\mathcal{Z}$ to each voxel $p \in \mathcal{P}$. The general energy function is given by

$$E(\mathbf{z}|\mathbf{I}) = \sum_{p \in \mathcal{P}} V_p(z_p|\mathbf{I}) + \sum_{p \in \mathcal{P}} \sum_{q \in \mathcal{N}_p} V_{p,q}(z_p, z_q|\mathbf{I}), \quad (9)$$

where $\mathbf{z}$ is a binary variable which defines the segmentation, $\mathbf{I}$ is the observed intensity data, $V_p(z_p|\mathbf{I})$ and $V_{p,q}(z_p, z_q|\mathbf{I})$ are the regional and the boundary terms respectively. The regional term encodes the individual penalties for assigning voxel $p$ to object and background given the observed image data $\mathbf{I}$. The boundary term encodes a discontinuity penalty between adjacent voxels $p, q$ incurred when they are jointly assigned labels $z_p$ and $z_q$ where $q \in N_p$ given the observed image data $\mathbf{I}$. They are based on the traditional graph-cut intensity based energy function of Boykov and Jolly [4].

### 3.1. Integrating Shape Prior Term

We propose to incorporate the additional shape prior term $V_p(z_p|\mathbf{x}^*)$ in the regional term of the energy functional $E(\mathbf{z}|\mathbf{I}, \mathbf{x}^*)$. The muscle segmentation problem is then solved by minimizing the modified energy functional given
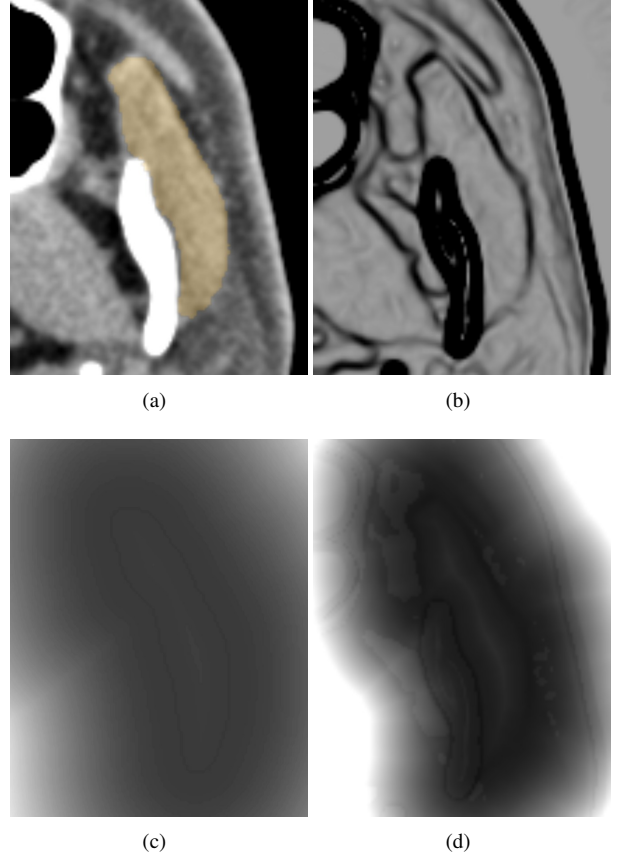


Figure 5. Dataset with ground truth (orange) in 2D (a), inverse edge map (b), unsigned distance map (c) and edge weighted unsigned distance map (d) (color online).

by

$$E(\mathbf{z}|\mathbf{I}, \mathbf{x}^*) = \sum_{p \in \mathcal{P}} \left\{ V_p(z_p|\mathbf{I}) + \mu V_p(z_p|\mathbf{x}^*) \right\}$$
$$+ \lambda \sum_{p \in \mathcal{P}} \sum_{q \in \mathcal{N}_p} V_{p,q}(z_p, z_q|\mathbf{I}), \quad (10)$$

where $\mathbf{x}^*$ is the optimal reconstructed shape which is used as the shape prior, $\lambda$ is the smoothness parameter and $\mu$ is the shape prior parameter. The shape term encodes how likely a particular voxel $p$ is to belong to the object "1" and the background "0", given the shape prior $\mathbf{x}^*$.

A probability map for the voxels to belong to the object and the background is created using the unsigned distance map of the shape prior's contour. All the voxels enclosed by the shape prior are used to create the object probability map. The voxels at the center of the shape are more likely to belong to the object as compared to the voxels close to the contour as shown in Fig. 4(a). Thus the voxels at the center incur a higher penalty to belong to the background as compared to voxels close to the contour. Voxels outside the contour incur 0 penalty for belonging to background.

The opposite is true for the background probability map, where only the voxels outside the contour are considered. The voxels close to the contour are more likely to belong to object as compared to the voxels farther away, see Fig. 4(b). The penalty is computed as the negative log-likelihood of belonging to object $V_p(z_p = \text{"1"}) = -\ln Pr(\mathbf{x}_p|\text{"1"})$ and background $V_p(z_p = \text{"0"}) = -\ln Pr(\mathbf{x}_p|\text{"0"})$. Such encoding of the global shape information transforms it into local constraints.

## 4. Implementation Details

In this section, we describe the implementation details for our masseter muscle segmentation. The Algorithm 1 along with Fig. 2 summarizes the steps of the proposed segmentation algorithm that are detailed in the upcoming subsection.

---

**Algorithm 1**

---

**Input**: Reconstruct optimal shape from landmarks.
**Output**: Graph-Cut segmentation of target muscle.
**Repeat**
- Compute $V_p(z_p|\mathbf{x}^*)$ as explained in Section 3.1.
- Create graph according to the energy function $E(\mathbf{z}|\mathbf{I}, \mathbf{x}^*)$.
- Segment using graph-cut.
- Create edge weighted unsigned distance map from segmentation.
- Optimize the shape model over this unsigned distance map.

**Until Convergence**

---

### 4.1. Initial Shape from the Landmarks

To get an initial estimation of the masseter muscle, procrustes method is used to align the statistical model with the given landmarks. In our case, we have six landmarks obtained manually. A reconstruction of the statistical model given the landmarks, as explained in Sec. 2.1, is then calculated to get an initial shape prior for the segmentation.

### 4.2. Shape Optimization

Once the initial shape has been determined, the shape probability maps for the object (see Fig. 4(a)) and the background (see Fig. 4(b)) are created as explained in Sec. 3.1. A graph $G$ corresponding to the energy function $E$ given by Eq. 10 is created and graph-cut [5] is used to compute the global minimum. The boundary of the resulting segmentation is then used to create an edge weighted unsigned distance map as shown in Fig. 5(d). This distance map is used as a cost function to fit the statistical shape model. Since the statistical shape model is represented by a very dense triangulated surface mesh, the vertices of the mesh

fall in voxels of the dataset and the corresponding value of the voxel given by the weighted unsigned distance map is the cost this vertex incurs given the shape coefficients $\boldsymbol{\alpha}$. The objective is to optimize the statistical shape model by minimizing the sum of the cost of vertices constrained by generating only statistically valid shapes. If the statistical model fits perfectly to the segmentation boundary, the cost of such a shape would be $0$. The coefficients of the main modes of variation $\boldsymbol{\alpha}$ of the statistical model are optimized using gradient descent based optimization approach. The optimized shape is then used as a shape prior for the next iteration to generate probability maps for the object and the background and the same process is iteratively applied until the convergence is reached (see Fig. 6).

### 4.3. Constraining The Variability

The theory of variability constrained statistical models (see Sec 2.2) is used during shape optimization as it is more stable as compared to the unconstrained statistical models. The vertices which are fixed at the known landmarks stay fixed or undergo only slight movement from their position; this avoids shrinking of the model. The generally used regularization scheme to constrain the model [3], forces the shape to be as close as possible to the mean shape $\bar{\mathbf{x}}$. Forcing a shape to be close to mean shape, however, decreases the flexibility of the statistical model to fully represent the shape variability of the anatomical structures. The benefit of smooth shapes comes at the cost of a reduced flexibility of the statistical model. It is also difficult to find good regularization parameters for each datasets. Using the statistical model with constrained variability in contrast provides a statistical model which is stable, generates smooth shapes and has reduced variability but no reduction in shape representational power of the model, because only the unnecessary variability has been removed. This constrained statistical model can still be regularized which will force the shape to be close to the optimal shape, as the optimal shape is also the mean shape of the constrained statistical model.

## 5. Experimental Results

The method was tested on 20 CT datasets of the masseter muscle with dataset dimensions 79-156 $\times$ 148-214 $\times$ 125-384 voxels and spacing 0.3-0.5 $\times$ 0.3-0.5 $\times$ 0.3-1 mm$^3$. All datasets were noisy, possessing mild to severe imaging artifacts such as high-density artifacts caused by *e.g.* the very common dental fillings and dental implants. The datasets were chosen randomly from the hospital repository so that they could represent anatomical variations. A medical expert provided the ground truth segmentations. Leave-One-Out approach was used to evaluate the method. The ground truth segmentations were used to create the statistical model with constrained variances. As it is difficult to pin-point the
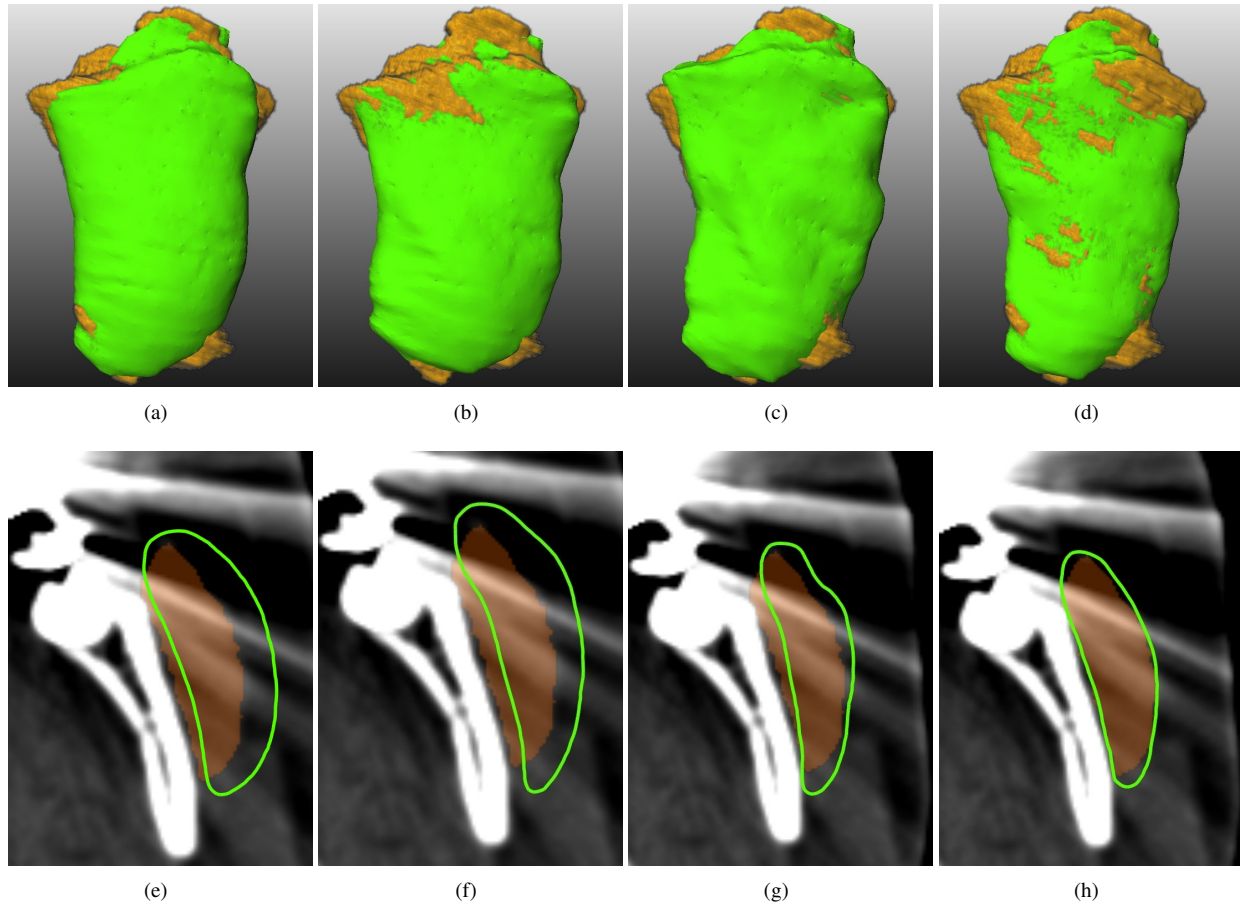
Figure 6. The evolution (left to right) of the shape prior (green) to the target muscle (orange) on a corrupted dataset. (a-d) in 3D and their corresponding 2D slices (e-h) (color online).
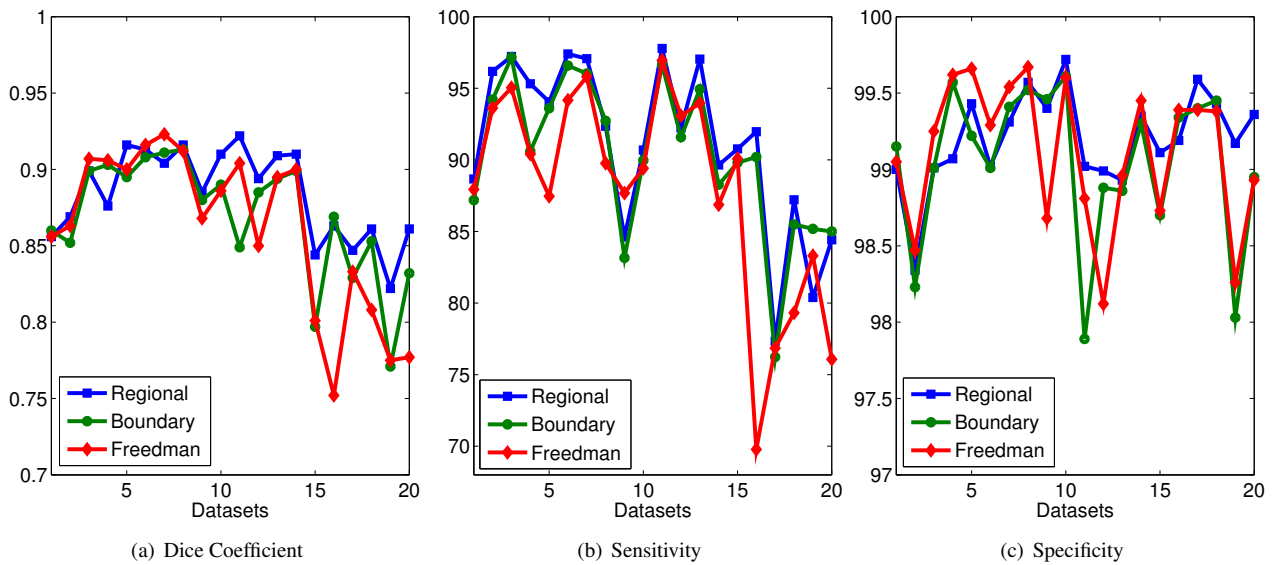


Figure 7. Comparison results. Incorporating the shape prior information in the regional term (blue) is more accurate as compared to methods that incorporate the shape in the boundary term (green and red). Note that the red curve shows the result of [10] where a fixed shape template is used in the boundary term (color online).

muscle attachments on the bone, the landmarks only provide a rough estimation of the location and the shape of the specific patient's muscle. The proposed technique, however, is unaffected by landmark placement and the model behaves nicely even when the landmarks have not been correctly placed. The statistical shape model converges to the target muscle shape in $4 - 7$ iterations. The segmentation time was around 5 minutes per dataset on a Ubuntu 11.04 PC (Intel(R) Core(TM) i7 CPU $8 \times 2.9$ GHz, 16 GB RAM, with OpenGL 4.1.0 and NVIDIA GeForce GTS 450 - 1GB RAM). The parameters $\sigma = 2.8$, $\lambda = 0.1$ and $\mu = 0.15$ were optimized on three different datasets and used throughout the entire segmentation experiments. The dice coefficient, sensitivity and specificity of the segmentation were calculated as similarity measures to ascertain the accuracy of the proposed method.
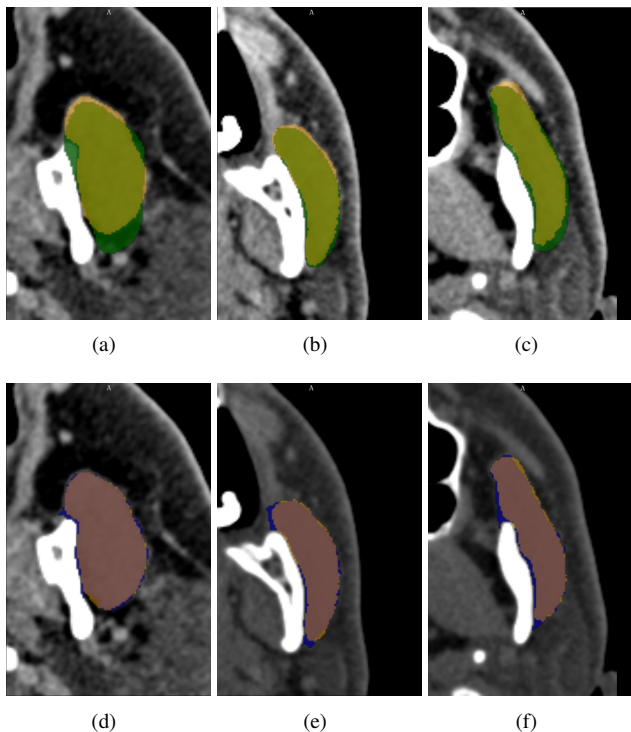


Figure 8. Shape prior and the segmentation result in 2D. (a-c) show shape prior (green) overlaid with ground truth (orange), while (d-f) show the segmentation (blue) (color online).

Figure 6 shows a shape update on one of the corrupted datasets. The ground truth has been shown in orange while the statistical shape model is shown in green. It can be seen in Fig. 6(e-h) that the statistical model shape update is robust to the high-density artifacts which corrupted the image data.

The graphs in Fig. 7 show the results of our method when the shape prior is added in the regional term (blue curve) and the boundary term (green curve). The proposed

method was also compared to the fixed shape template of Freedman and Zhang [10] (red curve) which also adds the shape prior in the boundary term. The results clearly show that the segmentation result by adding the shape prior in the regional term (blue curve) was more accurate than adding the shape prior in the boundary term (green curve), this was especially true for datasets (Datasets 15-20 in Fig. 7) with high-density artifacts. The shape prior in the boundary term has the effect of smoothing out regions which results in a portion of the muscle being smoothed out. This can be dealt with by incorporating the shape prior in the regional term which allows the flexibility to encode shape knowledge in areas where the intensity alone does not provide enough knowledge because of the artifacts. In such regions, the shape prior in the regional term can offset the intensity likelihood and estimate the likelihood of voxel belonging to the muscle based on the spatial location of the voxel with respect to the shape prior. This is the main motivation of adding a shape prior in the regional term.

Since Freedman and Zhang [10] use a fixed shape template as shape prior in the boundary term their results were worse than our results of adding the shape prior in the regional term especially for severely corrupted and noisy datasets. The reason being that a fixed shape template cannot adapt to the different anatomical shape variations of the muscle. Majeed *et al.* [13] has also used a fixed shape template both in the regional and the boundary terms with a 6-neighborhood system to segment the masseter muscle. We achieved higher segmentation accuracy as compared to Majeed *et al.* for the masseter muscle segmentation by employing a statistical model that accommodates higher shape variability and a 26-neighborhood system.

Figure 8 shows qualitative results of our technique in 2D, while the qualitative results in 3D are shown in Fig. 9. We have used a 26 neighborhood system which has resulted in better segmentation as compared to a 6 neighborhood system. The experimental results obtained using the proposed method are clinically acceptable as validated by the medical expert.

## 6. Conclusion

We have proposed a novel segmentation approach that combines a statistical shape model with an MRF-based segmentation framework, which is robust with respect to high-density artifacts. The statistical shape model was learned using a PPCA based approach which was instrumental in providing the model with a constrained variability. Using a constrained variability statistical model has proven to be a more sensible alternative for constraining the model. The shape knowledge provided as a triangulated surface mesh was transformed into the local shape constraints of the regional term of the MRF-based energy functional, and in the novel manner, the shape was updated over the edge
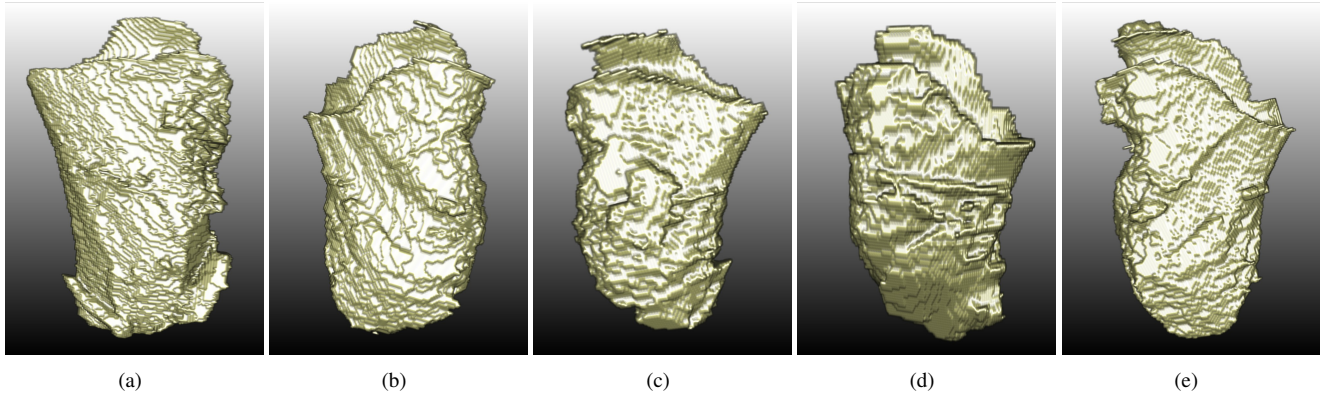
Figure 9. Segmentation result of the left (a-b) and the right muscles (c-e) in 3D.

weighted unsigned distance map in an iterative process. The method's performance was shown by segmenting the masseter muscle from CT datasets which is a challenging task because of the presence of soft tissues in close proximity as well as imaging artifacts. The results showed that by incorporating prior shape knowledge, clinically acceptable results can be achieved. In future work we plan to use higher order terms of the MRF-based energy functional to further increase the segmentation accuracy and to get smoother results.

## Acknowledgment

## References

[1] A. M. Ali, A. A. Farag, and A. S. El-Baz. Graph Cuts Framework for Kidney Segmentation with Prior Shape Constraints. In *MICCAI*, volume 10, pages 384–392, 2007.

[2] C. M. Bishop. *Pattern Recognition and Machine Learning*. Springer, 2nd edition, 2007.

[3] V. Blanz and T. Vetter. Reconstructing the Complete 3D Shape of Faces from Partial Information. In *Informationstechnik und Technische Informatik*, volume 44, pages 295–302, 2002.

[4] Y. Boykov and M.-P. Jolly. Interactive Graph Cuts for Optimal Boundary and Region Segmentation of Objects in N-D Images. In *ICCV*, volume 1, pages 105 – 112, 2001.

[5] Y. Boykov and V. Kolmogorov. An Experimental Comparison of Min-Cut/Max-Flow Algorithms for Energy Minimization in Vision. *PAMI*, 26(9):1124–1137, 2004.

[6] T. F. Cootes, C. J. Taylor, D. H. Cooper, and J. Graham. Active Shape Models; Their Training and Application. *Computer Vision and Image Understanding*, 61(1):38–59, 1995.

[7] P. Das, O. Veksler, V. Zavadsky, and Y. Boykov. Semi-Automatic Segmentation with Compact Shape Prior. *Image and Vision Computing*, 27(1):206–219, 2009.

[8] A. Dedner, M. Lüthi, T. Albrecht, and T. Vetter. Curvature Guided Level Set Registration using Adaptive Finite Elements. In *Pattern Recognition*, pages 527–536, 2007.

[9] N. El-Zehiry and A. Elmaghraby. Graph Cut Based Deformable Model with Statistical Shape Priors. In *ICPR*, pages 1–4, 2008.

[10] D. Freedman and T. Zhang. Interactive Graph Cut Based Segmentation with Shape Priors. In *CVPR*, pages 755–762, 2005.

[11] M. Freiman, A. Kronman, S. J. Esses, L. Joskowicz, and J. Sosna. Non-parametric Iterative Model Constraint Graph Min-Cut for Automatic Kidney Segmentation. In *MICCAI*, pages 73–80, 2010.

[12] M. Lüthi, T. Albrecht, and T. Vetter. Probabilistic Modeling and Visualization of the Flexibility in Morphable Models. In *Mathematics of Surfaces*, pages 251–264, 2009.

[13] T. Majeed, K. Fundana, M. Lüthi, J. Beinemann, and P. Cattin. A Shape Prior-Based MRF Model for 3D Masseter Muscle Segmentation. In *SPIE Medical Imaging*, 2012.

[14] J. Malcolm, Y. Rathi, and A. Tannenbaum. Graph Cut Segmentation with Nonlinear Shape Priors. In *ICIP*, volume 4, pages 365–368, 2007.

[15] G. G. Slabaugh and G. Unal. Graph Cuts Segmentation Using an Elliptical Shape Prior. In *ICIP*, pages 1222–1225, 2005.

[16] M. E. Tipping and C. M. Bishop. Probabilistic Principal Component Analysis. *Journal of the Royal Statistical Society*, 61(3):611–622, 1999.

[17] O. Veksler. Star Shape Prior for Graph-Cut Image Segmentation. In *ECCV*, volume 5304, pages 454–467, 2008.

[18] Volker Blanz and Thomas Vetter. A Morphable Model for the Synthesis of 3D Faces. In *Computer Graphics and Interactive Techniques*, pages 187–194, 1999.